Available online at www.sciencedirect.com

SciVerse ScienceDirect

Journal of Magnesium and Alloys 1 (2013) 82−87
www.elsevier.com/journals/journal-of-magnesium-and-alloys/2213-9567

Full length article

Investigation of a novel self-sealing pore micro-arc oxidation film on AM60 magnesium alloy

Yingwei Song*, Kaihui Dong, Dayong Shan, En-Hou Han

State Key Laboratory for Corrosion and Protection, Institute of Metal Research, Chinese Academy of Sciences, 62 Wencui Road, Shenyang 110016, China

Abstract

Micro-arc oxidation (MAO) is one of the promising methods to improve the corrosion resistance of magnesium alloys. However, there are plenty of micro-pores in the traditional MAO films, deteriorating their protection property. A novel self-sealing pore MAO film was developed in this paper. The morphologies and chemical composition of the film were detected by scanning electron microscopy (SEM) and energy dispersive X−ray spectroscopy (EDX). The corrosion behavior was investigated by electrochemical and salt spray tests. The possible film formation and corrosion mechanisms were proposed. The self-sealing pore film presents a blue appearance. Most of the micro-pores in the surface of the film are sealed during the film formation process. The chemical composition of the film mainly contains Mg, O, Ti, F and P. The self-sealing pore film exhibits better corrosion resistance compared with the traditional silicate film. Especially, the self-sealing pore film keeps intact after salt spray test for 2000 h, which can be attributed to its high compactness.

Keywords: Self-sealing pore; Micro-arc oxidation film; Magnesium alloy; Corrosion resistance

1. Introduction

Magnesium and its alloys have been widely used in the fields of automotive industry, electronic products, aerospace industry due to their special properties, such as low density, high strength-to-weight ratio, good castability, high damping capacity, good recycling potential and abundant resources. However, the usage of magnesium alloys is not yet widespread because their corrosion resistance is not adequate for many applications. Protective coatings are the most effective approach to improve the corrosion resistance. The common coatings include chemical conversion films, micro-arc oxidation (MAO) films, electroless plating coatings, organic coatings, PVD, laser cladding and so on [1−6]. Among these coatings, MAO films are the most promising because of their low cost, easy preparation, high corrosion and wear resistance and so on. Silicate, phosphate and aluminate electrolytes are three classical solutions for preparing MAO films [7−9]. The chemical composition of the films is composed of abundant MgO as well as a small amount of $MgSiO_3$, $Mg_3(PO_4)_2$ or $MgAl_2O_4$. However, plenty of micro-pores are visible within these MAO films. Corrosive electrolytes are susceptible to penetrating the films along these micro-pores [10]. As a result, the corrosion resistance of the MAO film degrades. Thus, current studies mainly focus on how to reduce the porosity. It is found that suitable electric parameters and novel electrolyte solutions are available for this aim. Srinivasan et al. [11] obtained a low porosity of the MAO film in silicate solution by using low current density. Liang et al. [12], Luo et al. [13] and Liu et al. [14,15] developed Zr-containing electrolytes to obtain the compact MAO films which consist of magnesium and zirconium oxides.

* Corresponding author. Tel.: +86 24 23915897; fax: +86 24 23894149.
E-mail address: ywsong@imr.ac.cn (Y. Song).

Peer review under responsibility of National Engineering Research Center for Magnesium Alloys of China, Chongqing University

Production and hosting by Elsevier

http://dx.doi.org/10.1016/j.jma.2013.02.009

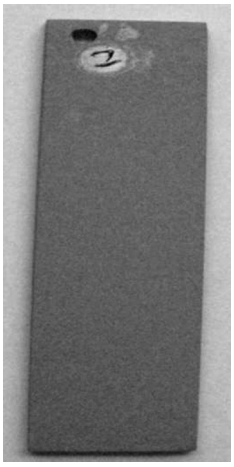

Fig. 1. Optical photo of the self-sealing pore film on AM60 Mg alloy.

Blawert et al. [16] reported that the clay particle addition to the solution can greatly decrease the number of micro-pores. Correspondingly, these compact MAO films exhibit better corrosion resistance than the traditional MAO films.

In this investigation, a novel Ti-containing electrolyte solution is developed to enhance the compactness of the MAO film. Especially, it is found that most of the micro-pores in the film are self-sealed during the film formation process. Also, the structure and corrosion behavior of the self-sealing pore film are investigated.

2. Experimental

The experimental material used for this investigation was cast AM60 magnesium alloy with a chemical composition (wt.%) of 5.89 Al, 0.53 Mn, 0.08 Zn, 0.003 Si, 0.002 Cu, 0.002 Ni, 0.004 Fe, and Mg balance. Samples with size of 60 × 30 × 2 mm were successively ground to 2000 grit silicon carbide papers, cleaned with alcohol, and then dried in cold air.

A 20 kW DC power supply was employed. The AM60 magnesium alloy samples were used as anodes and a stainless steel container was used as cathode during the MAO process. The electrolyte solution consists of 2 g L^{-1} $Na_5P_3O_{10}$, 6 g L^{-1} $(NaPO_3)_6$, 3 g L^{-1} NaOH and 10 g L^{-1} K_2TiF_6. The stainless steel container was put in a water-cooled bath in order to cool the electrolyte solution during the MAO treatment. The AM60 samples were immersed in this solution with a constant current density of 40 mA cm^{-2} until voltage reached 420 V and then kept this applied voltage for 2 min. The plus frequency and duty ratio were 1000 Hz and 30%, respectively.

The optical images of the MAO film were observed and taken photographs using a digital camera.

The microstructure and chemical composition were detected using a Phillips XL30 scanning electron microscopy (SEM) equipped with an energy dispersive X–ray spectroscopy (EDX).

The corrosion resistance was evaluated by electrochemical and salt spray tests. The electrochemical measurements were performed in 3.5 wt. % NaCl solution after an initial delay of 300 s using an EG&G potentiostat model 273 (Princeton Applied Research, Oak Ridge, TN, USA) and a model 5210 lock–in amplifier. A classical three–electrode cell was used, with a platinum plate as counter electrode, a saturated calomel electrode as reference electrode and the sample sealed with paraffin with an exposed area of 1 cm^2 as working electrode. The potentiodynamic measurements started from −200 mV below open circuit potential (OCP) at a constant scan rate of 0.5 mV s^{-1} and were terminated until a final current density of approximately 10 mA cm^{-2}. The polarization curves were fitted using CorrView software in the model of Tafel (Traditional), by intersecting the cathodic Tafel line and the level line at the OCP value. Electrochemical impedance spectroscopy (EIS) measurements were carried out under OCP. The scan frequency ranged from 100 kHz to 10 mHz with a perturbation amplitude of 10 mV. The plots were fitted using ZSimpWin software.

The salt spray test was carried out according to ASTM B117 standard (5 wt. % NaCl spray, 35 °C).

3. Results and discussion

3.1. Morphologies and chemical composition of the self-sealing pore MAO film

The optical photo of the self-sealing pore film on AM60 Mg alloy is shown in Fig. 1. The film presents a smooth blue surface. However, in the case of traditional MAO films, they present a white appearance [17]. The different color of the films

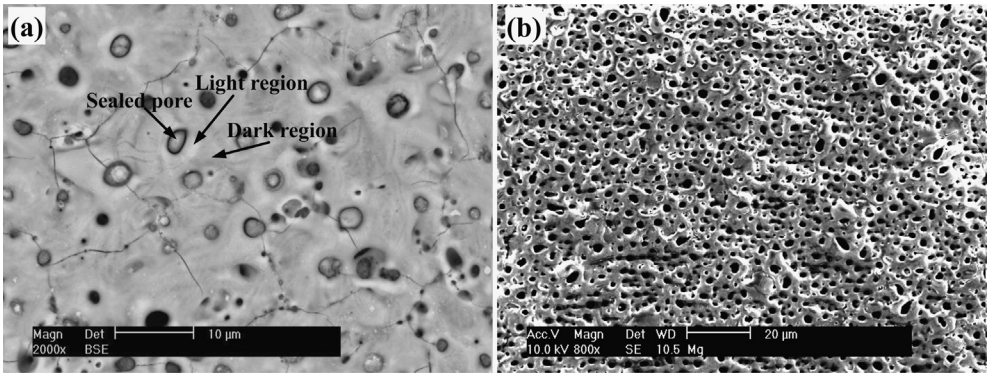

Fig. 2. Morphologies of the self-sealing pore film (a) and traditional silicate film (b).

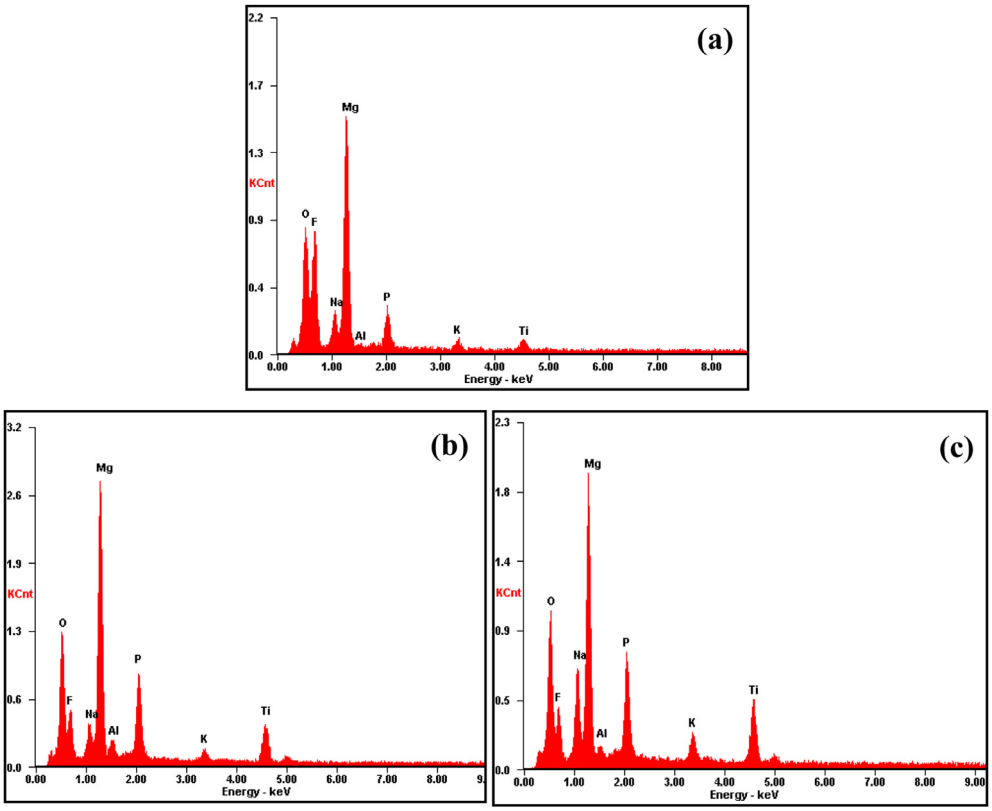

Fig. 3. EDX patterns of the sealed pore region (a) dark region (b) and light region (c) on the surface of the self-sealing pore film.

Table 1
Contents of the elements on various regions of the MAO film.

	O	F	Mg	P	Ti	Na	K	Al
Sealed pore	25.43	26.31	31.08	5.62	3.84	5.5	1.95	0.27
Dark region	28.25	11.57	29.13	11.01	9.7	6.19	1.99	2.16
Light region	28.36	9.77	24.61	10.34	13.85	8.24	3.78	1.05

implies that the chemical composition of the self-sealing pore film is possibly different from that of traditional MAO films.

Fig. 2a shows the SEM morphology of the self-sealing pore MAO film. Also, the morphology of the traditional silicate film prepared by Zhang [17] according to U.S. patent [18] is shown in Fig. 2b for the aim of comparing. It is found that plenty of micro-pores are visible on the surface of the traditional silicate film. These micro-pores display a uniform distribution with a dimension of below 5 μm. In the case of the self-sealing pores film, the diameter of the micro-pores varies in a large scope, from the largest one of approximately 3 μm to the smallest one of below 1 μm. Also, the quantity of the micro-pores is less. Especially, most of the micro-pores are sealed by some compounds, and only the very small micro-pores are open. It is obvious that the self-sealing pore film is more compact than the traditional silicate film. Moreover, the color distribution on the surface of the self-sealing pore film presents a slight difference. The regions around the sealed pores are brighter than that of far away from the sealed pores. The chemical composition of the sealed pore region, light region and dark region (marked in Fig. 2a) is analyzed by

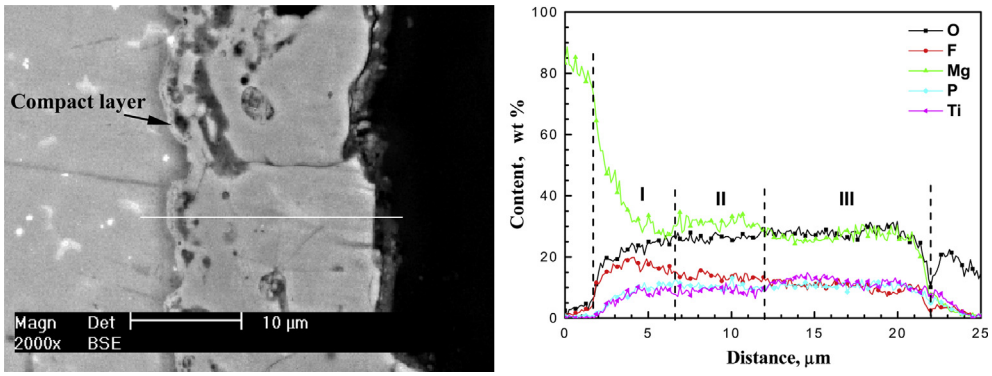

Fig. 4. Cross-section morphology and EDX line scan of the self-sealing pore film.

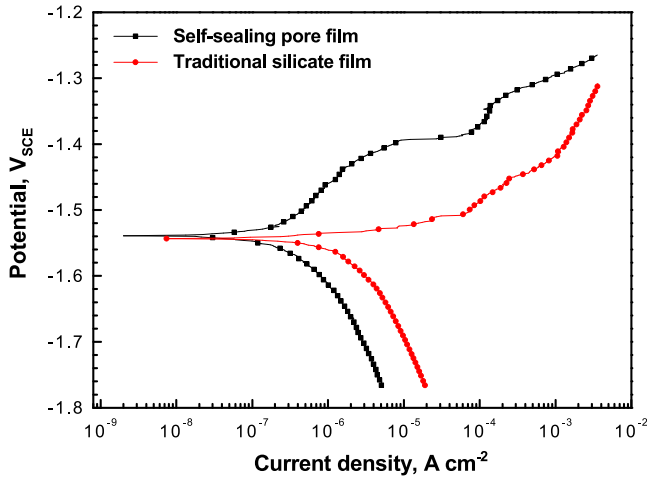

Fig. 5. Comparison of polarization curves between self-sealing pore film and traditional silicate film in 3.5% NaCl solution.

EDX as shown in Fig. 3. The contents of various elements are listed in Table 1. The three regions contain the same elements of O, F, Mg, P, Ti, Na, K and Al, but their contents are different. The elements of Mg and Al come from the Mg substrate, whereas the rest should come from the electrolyte solution. Especially, the elements of F, K and Ti root in the K_2TiF_6, implying that K_2TiF_6 occurs decomposition reaction during the film formation process. According to Table 1, the sealed pore region has the highest F content. Also, there exist abundant O and Mg. It means that the sealing pore compounds are mainly composed of magnesium oxides and fluorides. In comparison with the dark region, the light region contains more Ti but less Mg. The blue appearance of the film (Fig. 1) can be attributed to the existence of Ti_3O_5 which is a kind of bluish dark component.

Fig. 4a shows the cross-section morphology of the self-sealing pore film. The thickness of the film is approximately 20 μm. It is visibly a thin compact layer adhered to the Mg substrate. A thick loose layer locates on the compact layer. The main chemical composition of O, Mg, P and Ti along the cross-section of the film is analyzed by EDX line scan as shown in Fig. 4b. The film can be divided into three regions according to the chemical composition variations. In region I, the concentration of Mg element reduces sharply and the F element exhibits a higher concentration than that in region II and III. It indicates that fluorides enrich in the inner layer of the film. In comparison with region III, the region II contains more Mg but less Ti.

The possible film formation process can be proposed based on the morphology and chemical composition of the film. In the initial stage, a fluoride film can be preferentially formed in the electrolyte solution. The film becomes more compact with increasing film formation time, accompanying with the rise of voltage. Then the film will be broken down in the weak sites by high voltage to form spark channels. The components in the electrolyte solution can enter into the spark channels, and then is decomposed and form film under high temperature and

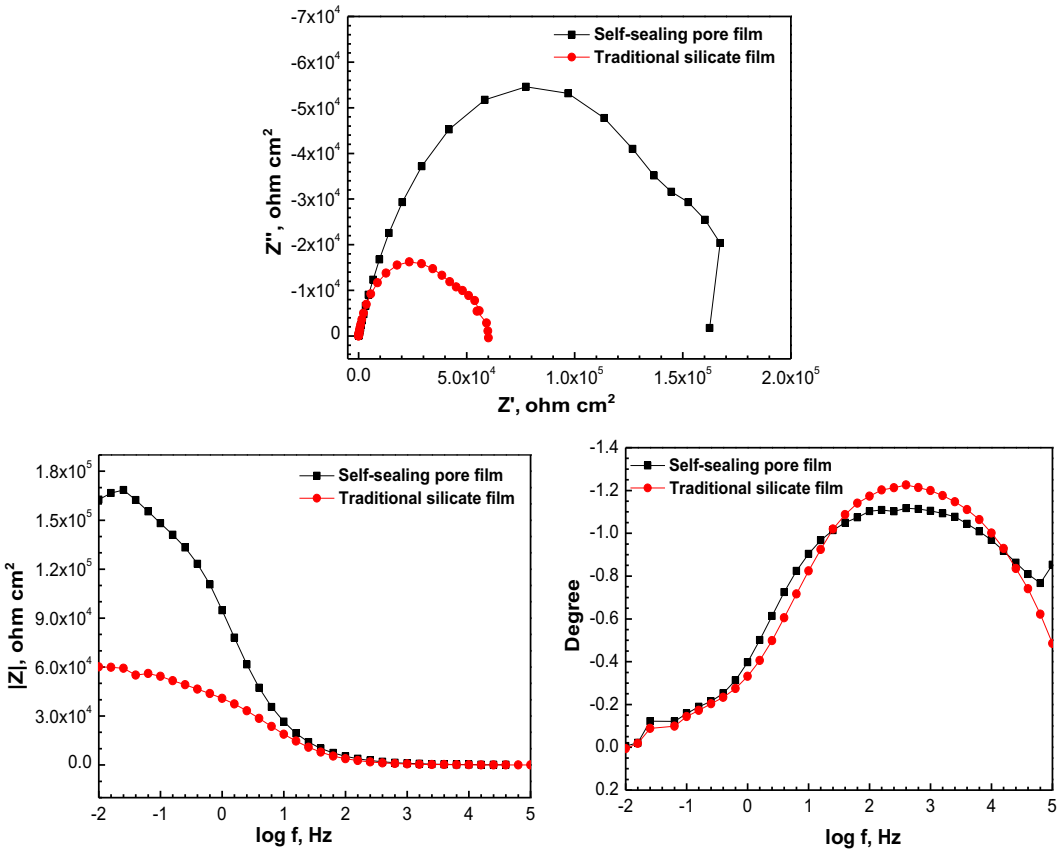

Fig. 6. Comparison of EIS plots between self-sealing pore film and traditional silicate film in 3.5% NaCl solution.

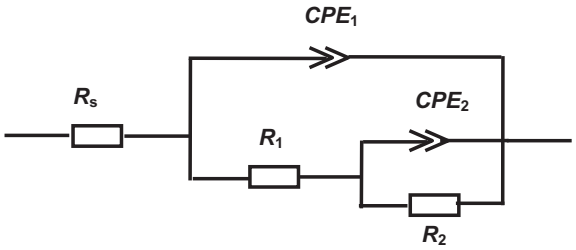

Fig. 7. Equivalent circuits of EIS plots for self-sealing pore film and traditional silicate film.

pressure condition. The above analysis is in agreement with the traditional MAO film. Differently, besides magnesium oxides and phosphates, fluorides and titanium oxides are formed in this film. The sintering temperatures of them are greatly different from that of magnesium oxides and phosphates. During the cooling process, the compounds of low sintering temperatures solidify later and just are deposited in the micro-pores, resulting in that the micro-pores are self-sealed during the film formation process.

3.2. Corrosion behavior of the self-sealing pore MAO film

Fig. 5 show the polarization curves of the self-sealing pore and traditional silicate films in 3.5% NaCl solution. Though the both curves exhibit nearly the same E_{corr} value of approximately −1.55 V vs. SCE, the shapes of the both curves show great difference. The cathodic sides are controlled by hydrogen evolution reaction, but the self-sealing pore film presents a lower hydrogen evolution rate. In the case of the anodic sides, there is an obvious passivation trend in the self-sealing pore film while quick dissolution reaction occurs in the traditional silicate film. The self-sealing pore film exhibits better protection property by inhibiting both the anodic and cathodic reactions. As a result, the i_{corr} value of the self-sealing pore film is nearly one order of magnitude lower than that of traditional silicate film. Thus, the polarization curves demonstrate that the self-sealing pore film is more effective to improve the corrosion resistance of magnesium alloys.

Fig. 6 shows the EIS plots of the self-sealing pore and traditional silicate films in 3.5% NaCl solution. The Nyquist plots both consist of one high frequency capacitance loop and low frequency capacitance loop, exhibiting the features of the external loose layer and inner compact layer, respectively [19]. But the diameter of the plot for self-sealing pore film is much larger than that of the traditional silicate film. Also, the Bode plots of |Z| vs. frequency indicate that the self-sealing pore film presents higher impedance value, which is nearly three times higher than that of traditional silicate film. Thus, the EIS results prove that the corrosion resistance of the self-sealing pore film is greatly superior to the traditional silicate film.

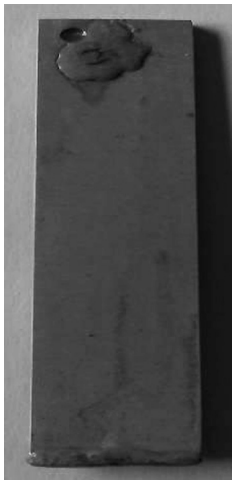

Fig. 8. Optical photo of the self-sealing pore film after salt spray test for 2000 h.

In order to further clarify the effect of the self-sealing pore MAO film on the corrosion resistance, the EIS spectra are analyzed based on the equivalent circuits shown in Fig. 7 and the fitting results are listed in Table 2. R_s represents the solution resistance. R_1 and R_2 represent the resistance of the external layer and inner layer of the MAO film, respectively. *CPE* (constant phase element) is used in place of a capacitor to compensate the non-homogeneity in the system, which is defined by two values, Y_0 and n. CPE_1 and CPE_2 relate to the capacity of the external layer and inner layer of the MAO film, respectively. The high frequency capacitance loop is described by R_1 and CPE_1, characterizing the external layer of the film. The low frequency capacitance loop is described by R_2 and CPE_2, characterizing the inner layer of the film. Based on the fitting results in Table 2, it can be found that the inner layer of the self-sealing pore film possesses much higher resistance value and lower capacity value than that of external layer, indicating that the inner layer of the film is more compact. In comparison with the traditional silicate film, both the inner layer and external layer of the self-sealing pore film present higher resistance value and lower capacity value. The EIS results indicate that the self-sealing pore film is more compact and corrosion resistant; especially the inner layer of the film plays a key role in hindering the corrosive electrolytes.

Also, the corrosion resistance of the self-sealing pore film is evaluated by salt spray test. Fig. 8 shows the optical photo of the self-sealing pore film after salt spray test for 2000 h. Corrosion pits are not observed on the surface of the film, but the color of the film is changed dramatically, from blue to grayish white. As analyzed before, the blue color can be associated with the existence of Ti_3O_5 in the film. After 2000 h salt spray test, the Ti_3O_5 in the surface layer of the film is dissolved, resulting in the variation of the color. As for the traditional MAO film, corrosive electrolytes can quickly

Table 2
Fitting results of EIS plots.

	R_s (Ω cm^2)	Y_{01} (Ω^{-1} cm^{-2} s^{-1})	n_1	R_1 (Ω cm^2)	Y_{02} (Ω^{-1} cm^{-2} s^{-1})	n_2	R_2 (Ω cm^2)
Self-sealing pores film	56.1	1.53×10^{-4}	0.915	2.95×10^{4}	9.53×10^{-8}	0.7141	1.50×10^{5}
Traditional silicate film	25	4.86×10^{-4}	0.764	1.57×10^{4}	1.56×10^{-6}	0.7898	4.44×10^{4}

penetrate the whole film along the micro-pores. Then corrosion occurs around the micro-pores. Usually, pitting corrosion and filiform corrosion are common for the traditional MAO films. In the case of the self-sealing pore film, the film is compact and most of the micro-pores are sealed during the film formation process. General corrosion occurs in the film during the salt spray test. The film will gradually dissolve and degrade from surface to the inner layer. Consequently, the self-sealing pore film can keep intact for long duration.

4. Conclusions

A novel Ti-containing electrolyte solution is used to obtain the self-sealing pore MAO film. The sealing pore components mainly consist of magnesium oxides and fluorides. Besides magnesium oxides and phosphates, titanium oxides are detected in the film. The film presents a blue appearance, which is attributed to the existence titanium oxides. In addition, the concentration of the fluorides is higher in the inner layer of the film. Also, the inner layer is more compact than the external layer. The formation of self-sealing pores is mainly associated with the various sintering temperature of the components in the film.

The polarization curves and EIS plots show the same results that the corrosion resistance of the self-sealing pore film is much superior to the traditional silicate film. Especially, the inner layer of the self-sealing pore film plays a key role in improving the protection property. General corrosion occurs in the self-sealing pore film during salt spray test, which can be attributed to the more compact of the film. The self-sealing pore film can provide perfect protection to the magnesium alloy substrate.

Acknowledgments

The authors thank the financial support by the National Natural Science Foundation of China (No. 51171198), National Key Basic Research Program of China (No. 2013CB632205) and the International Science & Technology Cooperation Program of China (2011DFA50904).

References

[1] Y.W. Song, D.Y. Shan, E.H. Han, Electrochim. Acta 53 (2008) 2135−2143.
[2] R.F. Zhang, D.Y. Shan, R.S. Chen, E.H. Han, Mater. Chem. Phys. 107 (2008) 356−363.
[3] Y.W. Song, D.Y. Shan, R.S. Chen, F. Zhang, E.H. Han, Surf. Coat. Technol. 203 (2009) 1107−1113.
[4] Y.L. Gao, C.S. Wang, H.J. Pang, H.B. Liu, M. Yao, Appl. Surf. Sci. 253 (2007) 4917−4922.
[5] H. Altun, S. Sen, Mater. Des. 27 (2006) 1174−1179.
[6] H.W. Shi, F.C. Liu, E.H. Han, Prog. Org. Coat 66 (2009) 183−191.
[7] H.F. Guo, M.Z. An, H.B. Huo, S. Xu, L.J. Wu, Appl. Surf. Sci. 252 (2006) 7911−7916.
[8] Y.Y. Ma, H. Hu, D. Northwood, X.Y. Nie, J. Mater. Process. Technol. 182 (2007) 58−64.
[9] A. Ghasemi, V.S. Raja, C. Blawert, W. Dietzel, K.U. Kainer, Surf. Coat. Technol. 202 (2008) 3513−3518.
[10] S.L. Wang, C.X. Pan, Q.Z. Cai, B.K. Wei, J. Chin. Soc. Corros. Prot. 28 (2008) 219−224 (in Chinese).
[11] P.B. Srinivasan, J. Liang, C. Blawert, M. Stormer, W. Dietzel, Appl. Surf. Sci. 255 (2009) 4212−4218.
[12] J. Liang, P.B. Srinivasan, C. Blawert, W. Dietzel, Corros. Sci. 51 (2009) 2483−2492.
[13] H.H. Luo, Q.Z. Cai, B.K. Wei, B. Yu, J. He, D. j. Li, J. Alloys. Compd. 474 (2009) 551−556.
[14] F. Liu, D.Y. Shan, Y.W. Song, E.H. Han, W. Ke, Corros. Sci. 53 (2011) 3845−3852.
[15] F. Liu, D.Y. Shan, Y.W. Song, E.H. Han, Surf. Coat. Technol. 206 (2011) 455−463.
[16] C. Blawert, S.P. Sah, J. Liang, Y.D. Huang, D. Höche, Surf. Coat. Technol. 213 (2012) 48−58.
[17] R.F. Zhang, Study of Anodization and Galvanic Corrosion in Magnesium Alloys, Ph.D. thesis, Institute of Metal Research, Chinese Academy of Sciences, 2005 (in Chinese).
[18] D.E. Bartak, B.E. Lemieux, E.R. Woolsey, Hard Anodic Coating for Magnesium Alloys, U.S. Patent: 5470664, 1995.
[19] H.P. Duan, K.Q. Du, C.W. Yan, F.H. Wang, Electrochim. Acta 51 (2006) 2898−2908.